Performance Simulation of the JPL Solar-Powered Distiller Part I. Quasi-Steady-State Conditions

C. S. Yung and F. L. Lansing
DSN Engineering

A 37.85-m^3 (10,000 gallons) per year (nominal) passive solar-powered water distillation system has been installed and is operational in the Venus Deep Space Station at Goldstone, California. The system replaced an old, electrically powered water distiller. The distilled water produced with its high electrical resistivity is used to cool the sensitive microwave equipment. A detailed thermal model has been developed to simulate the performance of the distiller and study its sensitivity under varying environment and load conditions. The quasi-steady-state portion of the model is presented together with the formulas for heat and mass transfer coefficients used. Initial results indicated that a daily water evaporation efficiency of 30% can be achieved. A comparison made between a full day performance simulation and the actual field measurements gave good agreement between theory and experiment, which verified the model.

I. Introduction

A 37.85-m^3 nominal (10,000 gallons) per year passive solar-powered distillation (solar still) system has been operating successfully in the Venus station (DSS 13) of the Deep Space Network (DSN) tracking complex at Goldstone, California, since the initial installation in December 1981. Although this solar still system was intended to be an experimental system, only a few problems have been encountered. Those problems were minor and were corrected without impairing the operation of the system. Continuous observation of the installed system has indicated that it is highly productive, requiring only minimum maintenance. The potential application of similar solar-powered distillers in other DSN stations is being examined to replace present electrically powered distillation systems.

In order to complement the experimental investigation, a detailed analytical model of the solar still module is developed. This report presents the quasi-steady-state portion of the model to simulate the module performance in a simple, yet accurate manner. A computer program was written using the model characteristic equations to speed up the parameterization study.

A literature search was made earlier (Refs. 1-4) to gather available information on existing simulation tools for solar-distillation systems. Dunkle (Ref. 1) appeared to be a pioneer researcher on solar-stills. The steady-state solution was tried by Dunkle (Ref. 1) and Morse and Read (Ref. 2). Sayigh (Ref. 3) presented a gross steady-state model of solar still, neglecting the internal heat exchanges and the influence of

makeup water. Cooper (Ref. 4) presented a transient model where heat flow to the ground beneath the still was strongly emphasized. A finite-difference method was used to determine the temperature distribution below the ground surface. The multiple reflections between the glass and the water were not considered in the model.

In order to provide an accurate simulation of the JPL solar distiller, the model is developed based on the JPL design configuration (Ref. 5) and includes all the influencing factors such as multiple reflections effect, internal heat exchange, and makeup water.

II. Design Details

Figure 1 illustrates the design details (Ref. 5) of the JPL solar distillation module. The system consists of 8 modules. The still module consists of a molded fiberglass tray with glass glazing on top sealed with special silicone rubber (RTV). The bottom of the still module is insulated with rigid foam and reinforced with marine plywood. The base of the wetted tray is painted black to serve as the solar absorber for evaporation enhancement. The remaining interior surface of the tray is colored white to promote reflection of sunlight into the water layer. The solar still is mounted on a welded steel frame elevated 3.35 m (11 ft) above ground level to facilitate the gravity feed and to eliminate shading caused by nearby structures. The solar still is oriented due south for maximum solar exposure.

Local well water with a high mineral content is supplied to the solar still by gravity from a storage tank located on a hill 91 m (300 ft) above the solar still inlet. The distilled water is collected in a 322-liter (85 gallon) temporary holding tank and then released to a large 5.7-m^3 (1500-gallon) underground storage tank for use in the microwave klystron-tube cooling system.

III. Model Assumptions

The following assumptions are made for a one-dimensional thermal model.

(1) The thermal losses from all four sides of the still module are neglected due to the presence of side air gaps. The side surfaces are painted a light color which enhances the reflection of the incoming solar radiation toward the water body. The sides temperature is assumed to be identical to the internal air temperature, with negligible heat loss to the ambient air.

(2) The distillation mechanism is viewed as follows: natural convection takes place while the water vapor is diffused uniformly from the water surface at T_w through the air space and condenses at the glass temperature T_g. The bottom surface of the still is painted black and absorbs most solar energy received.

(3) Due to the small inclination angle of the glass cover, the optical effect of the system is modeled as two parallel transparent media with an opaque bottom surface for the bottom medium.

(4) The internal air space is assumed to be 100% transparent to solar energy. No air leakage is assumed to take place to or from the solar still.

IV. Quasi-Steady-State Model

Using the above assumptions, a quasi-steady-state model has been developed; the details of the heat balance equations are presented in Appendix A. Appendix B gives the details of the heat transfer coefficients used in the model. Appendix C gives the mass transfer and diffusion coefficients. Appendix D illustrates the model use by a numerical example. Since the heat capacitance of the solar still components is not included in a steady-state solution, only the glass cover, the water layer, and the bottom layer of the fiberglass tray are included. From Eqs. (A.8), (A.15), and (A.17), the temperatures of these three components are expressed as:

$$T_w = [(B_1 + B_2 + m_w C_w)\, T_g - (E_1 + B_1 T_0)]/(B_2 + m_w C_w)$$

$$T_f = (E_3 + h_{c,fw} T_w)/B_4 \qquad (1)$$

$$T_g = (X_0 + X_1 T_0 + X_2 T_m)/(X_1 + X_2)$$

where the B's are equivalent heat transfer coefficients and the X's are characteristic constants that depend on the evaporation rate, thermal conductance, and the solar absorptivity of various components. Detailed descriptions of the B's and X's are given in Appendix A.

The nonlinearities in the radiation energy and water diffusion terms make the equations difficult to solve explicitly. An iteration method was used to obtain the final solution which uses a set of initially given temperatures: T_g, T_w and T_f, for the glass cover, the water layer, and the fiberglass bottom, respectively. The temperature-dependent terms such as the Grashof number Gr, saturated vapor pressure P_w, latent heat of evaporation of water L, heat convection coefficients for air and water, and the linearized radiation heat transfer coefficients can be calculated. The new set of temperatures can be determined using Eq. (1). By recomputing the temperature-dependent parameters using the new temperatures, a more

accurate set of temperatures can be determined, and the procedure is repeated until convergence is reached.

V. Evaporation Rate

Water evaporates isothermally from the top surface of the water layer at temperature T_w and diffuses upward through the stagnant air layer to the glazing. Water vapor condenses on the interior surface of the glazing at a lower temperature T_g. This diffusion process is caused by the differential saturated water vapor pressures in the air layer, at the boundary of the water layer, and at the boundary of the glazing. The evaporation rate of water, per unit still area m_w, is given in Appendix C as

$$m_w = \frac{DPM_w}{\bar{R}T_a\delta_a} \ln \frac{(P - P_{wg})}{(P - P_{ww})} \tag{2}$$

where D is the diffusion coefficient (m^2/hr), P is the system pressure (N/m^2), M_w is the molecular weight of water, $\bar{R}$ is the universal gas constant, δ_a is the average air spacing between the water surface and the glass cover, and P_{wg} and P_{ww} are the saturated water pressure at the glass temperature and the water temperature, respectively.

If the leakage of air and water vapor is assumed negligible, the amount of water produced by evaporation-condensation would be completely replenished by the makeup water at an inlet temperature T_m. Hence, Eq. (2) represents the amount of water evaporation rate or the makeup water rate.

VI. Distillation Efficiency

The instantaneous (or steady-state) distillation efficiency based on a constant solar radiancy on the projected area is defined by

$$\eta = \frac{m_w L}{I} \tag{3}$$

where L is the heat of vaporization of water. In general, the evaporation efficiency increases with increasing the solar energy intensity where it reaches maximum efficiency at noon. Although the instantaneous (or steady-state) efficiency gives an indication of the system performance under constant environmental conditions, it is not a complete characterization of the distiller performance over a full day or a year period. The other alternative to an accurate transient similation is to have a sequence of 24-hour quasi-steady-state simulation for each day. Accumulated daily efficiency can be obtained by dividing the accumulated distilled water production up to time t by the accumulated solar incident energy up to time t; i.e.,

$$\eta(t) = \sum_0^t m_w(t) L \Big/ \sum_0^t I(t) \tag{4}$$

VII. Simulation Results

In order to facilitate the simulation process, a computer program was written to speed up the analysis of the system under many different operating conditions. Appendix D gives a sample one-hour simulation. When the sample solar still module operates at 299.85 K (~80°F) ambient temperature with 800 W/m^2 of solar intensity, it would yield 0.73 kg/hr (0.19 gal/hr) of distilled water. The temperature of the glass cover, water layer, and the bottom surface would be 317.1 K (111°F), 343.8 K (159.2°F), and 347.2 K (165.30°F), respectively. The steady-state or instantaneous efficiency would be 28.6%.

An experimental measurement program was conducted on the JPL solar still to determine its actual performance. Under a solar intensity of about 800 W/m^2 and 32°C (89.6°F) ambient temperatures, the measured water temperature was approximately 71°C (159°F). With this actual field measurement in good agreement with quasi-steady-state simulations, we proceeded using the model to determine the effect of the major solar still performance parameters.

In addition to an instantaneous performance simulation, a full-day simulation was performed for the month of June 1982 to predict the daily distilled water production rate. In the full-day simulation, the hourly solar intensities are calculated by using the ASHRAE model (Ref. 6) on an average day on June 21 at Goldstone, California (latitude is 35°N). The outdoor air temperature profile was measured and the wind speed is assumed to be constant for the day at 4.47 m/sec (10 miles/hr). Since in a full-day simulation, steady-state conditions are assumed to be reached at the end of each hour of operation, the summation of the hourly water production rate would give the accumulated daily water production. The results of the full-day simulation of the JPL design indicated that the water production during 12 sunshine hours (from 6:00 a.m. to 6:00 p.m.) in June would yield 61.3 kg/day (16.2 gallons/day) of purified water vs the measured 64 kg/day (17 gallons/day), representing a 4.2% difference between the two values. Part of this deviation could be due to applying the quasi-steady-state method instead of the true transient method. Water production trails the solar intensity profile by a time-

lag. Errors in estimating material optical and thermal properties are responsible for another part of the deviation. The idealization and the assumptions listed in Section III contribute to the rest of the deviation.

A graphical presentation of the daily performance of one solar-powered distillation module for the month of June is given in Fig. 2. As shown in this graph, the water purification rate reached a peak value of 1.11 kg/hr (or 0.53 kg/(hr-m^2)) at noon, representing a maximum instantaneous efficiency of 35%. Since the measured daily temperature profile was higher in the afternoon than in the morning, the module produced larger quantities of distilled water in the afternoon. The accumulated efficiency increased asymptotically to 29.7% at 2:00 p.m. and then dropped slightly to give a daily efficiency of 29.1% as a typical daily efficiency in June.

In addition to the above quasi-steady-state model, which provides accurate simulation, a transient model and a detailed sensitivity study are planned for the distiller. The results of the comparison between quasi-steady and transient simulations and parameterization will be presented in a future report.

Acknowledgment

The authors are indebted to F. W. Stoller, D. Kuma, R. Z. Toukdarian, and F. Menninger for their technical management in the implementation of the JPL solar still at the Venus Deep Space Station. Acknowledgement is extended to R. Elder and J. May for providing valuable experimental data on weather and water purification rates.

References

1. Dunkle, R. V., "Solar Water Distillation: The Roof Type Still and a Multiple Effect Diffusion Still," paper presented at the 1961 International Heat Transfer Conference, University of Colorado, Boulder, Colo., Part 5, pp. 895-902, 1961.
2. Morse, R. N., and Read, W. R. W., "A Rotational Basis for the Engineering Development of a Solar Still," *Solar Energy*, Vol. 12, pp. 5-17, 1968.
3. Sayigh, A. A. M., Elsalam, E. M. A., "Optimum Design of a Single Slope Solar Still in Riyadh, Saudi Arabia," AIAA Paper No. A77-42956, Technical Information Service, New York, N.Y., 1977.
4. Cooper, P. I., "Digital Simulation of Transient Solar Still Processes," *Solar Energy*, Vol. 12, pp. 313-331, 1969.
5. Menninger, F. J., and Elder, R. J., "A Solar-Powered Water Purification System at Goldstone DSS 13," *TDA Progress Report 42-66*, Jet Propulsion Laboratory, Pasadena, Calif., pp. 352-354, Dec. 15, 1981.
6. *ASHRAE Handbook of Fundamentals*, American Society of Heating, Refrigerating and Air-Conditioning Engineers, Inc., New York, 1972.
7. Lansing, F. L., and Yung, C. S., "A Two-Dimensional Thermal Analysis of a New High Performance Tubular Solar Collector," *DSN Progress Report 42-49*, Jet Propulsion Laboratory, Pasadena, Calif., pp. 116-131, Feb. 15, 1979.

8. Holman, J. P., *Heat Transfer*, McGraw Hill Book Co., New York, N.Y., 1981.

9. Siegel, R., and Howell, J. R., *Thermal Radiation Heat Transfer*, McGraw-Hill Book Co., New York, 1972.

10. Eckert, E. R. G., and Drake, R. M., *Analysis of Heat and Mass Transfer*, McGraw-Hill Book Co., New York, 1972.

11. Duffie, J. A., and Beckman, W. A., *Solar Energy Thermal Processes*, Wiley Interscience Publication, New York, 1973.

12. Keenan, J. H., and Keys, G., *Thermodynamic Properties of Steam*, Wiley, New York, 1936.

List of Symbols

A	surface area
C	specific heat
D	water vapor, air diffusion coefficient
F	radiation view factor
g	gravitational constant
Gr	Grashof number
h_c	convective heat transfer coefficient
h_d	mass transfer coefficient
H'	enthalpy of saturated water liquid
H''	enthalpy of saturated water vapor
I	solar radiation intensity
k	thermal conductivity
l	characteristic length
L	latent heat of vaporization
Le	Lewis number
m	rate of makeup water or distilled water per unit area
M	molecular weight
Nu	Nusselt number
P	pressure
Pr	Prandtl number
$\overline{R}$	universal gas constant
Sc	Schmidt number
Sh	Sherwood number
t	time
T	absolute temperature
V	wind speed
X	constants
α	absorptivity
$\overline{\alpha}$	thermal diffusivity
β	volumetric expansion coefficient
δ	thickness
ϵ	emissivity
η	efficiency
μ	dynamic viscosity
ν	kinematic viscosity
ρ	reflectivity
$\overline{\rho}$	density
σ	Stefan Boltzman constant
τ	transmissivity
ϕ	extinction coefficient

Subscripts

a	airspace between glass and water
c	convection
e	effective
f	bottom fiberglass
g	glass
i	bottom insulation
o	ambient air
r	radiation
s	bottom plywood support
w	water

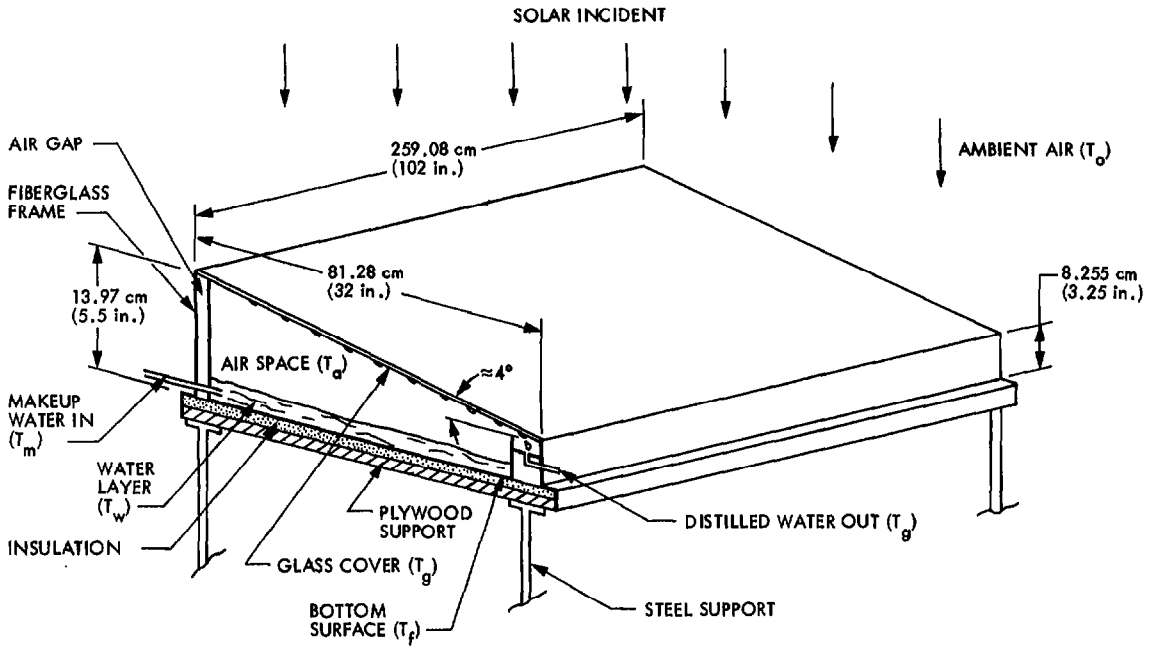

Fig. 1. Layout of JPL solar-powered distillation module

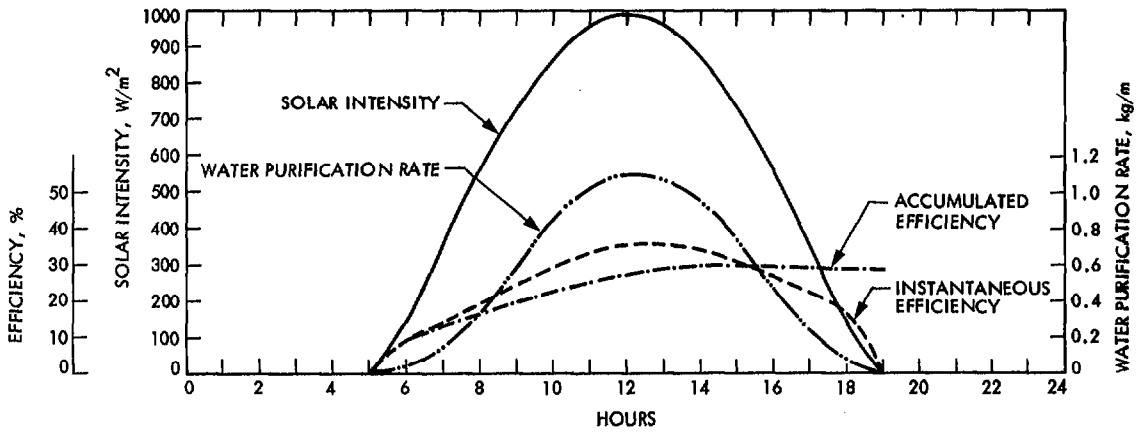

Fig. 2. Daily performance of one module in June

Appendix A
Derivation of Quasi-Steady-State Equations

The derivations of the governing heat and mass transfer equations for the quasi-steady state conditions are made following the assumptions outlined in Section III. The heat transfer coefficients are given in Appendix B and the mass transfer coefficients are given in Appendix C. Figure A-1 depicts the energy flow to and from the major components: the glass cover, the water layer and the bottom of the still.

A. Optical Properties

The optical effect of the glass cover and the water layer of the solar still can be modeled as two parallel transparent media with an opaque bottom surface for the second medium representing the black interior bottom of the still. The expressions of the "effective" absorptivity, reflectivity, and transmissivity due to multiple ray reflections are taken from Ref. 7 as follows.

For the glass cover, the effective absorptivity is

$$\left.\begin{aligned} \alpha_{g,e} &= \alpha_g + \frac{\alpha_g \tau_g \rho_w}{1-\rho_g \rho_w} \\ \text{for the water layer} \\ \alpha_{w,e} &= \alpha_w \tau_g/(1-\rho_g \rho_w) \\ \text{for the bottom surface} \\ \alpha_{f,e} &= \alpha_f \tau_g/(1-\rho_g \rho_w) \end{aligned}\right\} \quad \text{(A-1)}$$

where the single-layer absorptivities $\alpha_g, \alpha_w, \alpha_f$ for the glass cover, water layer, and the bottom surface, respectively, are given by the expressions

$$\left.\begin{aligned} \alpha_g &= (1-r_g)(1-a_g)/(1-a_g r_g) \\ \alpha_w &= (1-r_w)(1-a_w)(1+a_w b)/(1-a_w^2 b r_w) \\ \alpha_f &= a_w(1-b)(1-r_w)/(1-a_w^2 b r_w) \end{aligned}\right\} \quad \text{(A-2)}$$

where r_g and r_w are the ray reflection coefficient from the upper surface of glass and water respectively, b is the reflection coefficient of the opaque bottom surface of water and a is the ray absorption coefficient determined by

$$\left.\begin{aligned} a_g &= e^{-\phi_g \delta_g} \\ a_w &= e^{-\phi_w \delta_w} \end{aligned}\right\} \quad \text{(A-3)}$$

where ϕ is the extinction coefficient (in m^{-1}). Note that the reflectivities for the glass cover ρ_g and for the water layer ρ_w are computed from

$$\left.\begin{aligned} \rho_g &= r_g + \frac{r_g a_g^2 (1-r_g)^2}{(1-r_g^2 a_g^2)} \\ \rho_w &= r_w + [a_w^2 b (1-r_w)^2]/(1-a_w^2 b r_w) \end{aligned}\right\} \quad \text{(A-4)}$$

By using Eqs. (A-2) and (A-4), the transmissivity of the glass cover τ_g must satisfy the energy equation

$$\tau_g = 1 - \rho_g - \alpha_g \quad \text{(A-5)}$$

B. Heat Balance Equations

Figure (A-1) depicts the energy flux to and from the still components. At steady-state conditions the heat balance equations are divided as follows:

1. The glass cover. By selecting a control volume as shown in Fig. A-2, the energy balance equation is

$$\begin{aligned} &\alpha_g I + m_w H''_{Tw} + (h_{c,wg} + h_{r,wg})(T_w - T_g) \\ &= (h_{c,go} + h_{r,go})(T_g - T_o)\left(\frac{A_g}{A_w}\right) + m_w H'_{Tg} \end{aligned} \quad \text{(A-6)}$$

where m_w is the mass flow rate of water per unit area, and I is the solar radiation intensity on the projected area of glass cover A_g (which is equal to the water surface area A_w). The enthalpy terms can be combined as

$$H''_{Tw} - H'_{Tg} = L_{Ta} + C_w (T_w - T_g) \quad \text{(A-7)}$$

where L_{Ta} is the latent heat of vaporization evaluated at the internal air space temperature T_a. T_a is taken as the average

temperature between T_w and T_g. Combining Eqs. (A-6) and (A-7) gives

$$T_w = [(B_1 + B_2 + m_w C_w)\, T_g - (E_1 + B_1 T_o)]/(B_2 + M_w C_w) \tag{A-8}$$

where

$$\left.\begin{aligned} B_1 &= (h_{c,go} + h_{r,go})(A_g/A_w) \\ B_2 &= h_{c,wg} + h_{r,wg} \\ E_1 &= \alpha_g I + m_w L_{Ta} \end{aligned}\right\} \tag{A-9}$$

2 **The water layer.** For the water layer, the energy equation can be derived by using the control volume as shown in Fig. A-2 as

$$\alpha_w I + h_{c,fw}(T_f - T_w) + m_w H'_{Tm} = (h_{c,wg} + h_{r,wg})(T_w - T_g) + m_w H''_{Tw} \tag{A-10}$$

where H'_{Tm} is the enthalpy of the make up water at T_m, and H''_{Tw} is the enthalpy of the saturated water vapor at T_w. The difference in enthalpy $(H''_{Tw} - H'_{Tm})$ can be written as

$$H''_{Tw} - H'_{Tm} = L_{Tw} + C_w (T_w - T_m) \tag{A-11}$$

where L_{Tw} is the latent heat of vaporization of water at T_w (or taken at T_a approximately). Equations (A-10) and (A-11) give the temperature T_f as

$$T_f = (B_3 T_w - B_2 T_g - E_2)/h_{c,fw} \tag{A-12}$$

where

$$\left.\begin{aligned} B_3 &= h_{c,fw} + B_2 + m_w C_w \\ E_2 &= \alpha_w I + m_w C_w T_m - m_w L \end{aligned}\right\} \tag{A-13}$$

3. **Bottom fiberglass surface.** For the bottom fiberglass surface

$$\alpha_f I = h_{c,fw}(T_f - T_w) + h_{fo}(T_f - T_o) \tag{A-14}$$

or

$$T_f = (E_3 + h_{c,fw} T_w)/B_4 \tag{A-15}$$

where

$$\left.\begin{aligned} B_4 &= h_{c,fw} + h_{fo} \\ E_3 &= \alpha_f I + h_{fo} T_o \end{aligned}\right\} \tag{A-16}$$

By manipulating Eqs. (A-8), (A-12), and (A-15), the temperature T_g can be expressed as

$$T_g = (X_0 + X_1 T_0 + X_2 T_m)/(X_1 + X_2) \tag{A-17}$$

where

$$X_0 = (m_w L + \alpha_g I)\left[\frac{h_{c,fw}\, h_{fo}}{h_{c,fw} + h_{fo}}\right] + I(B_2 + m_w C_w)\left[\alpha_g + \alpha_w + \left(\frac{\alpha_f h_{c,fw}}{h_{c,fw} + h_{fo}}\right)\right] \tag{A-18}$$

$$X_1 = (B_1 + B_2 + m_w C_w)\left[\frac{h_{c,fw}\, h_{fo}}{h_{c,fw} + h_{fo}}\right] + B_1 (B_2 + m_w C_w)$$

$$X_2 = m_w C_w (B_2 + m_w C_w)$$

where the latent heat L is taken at the air space temperature T_a.

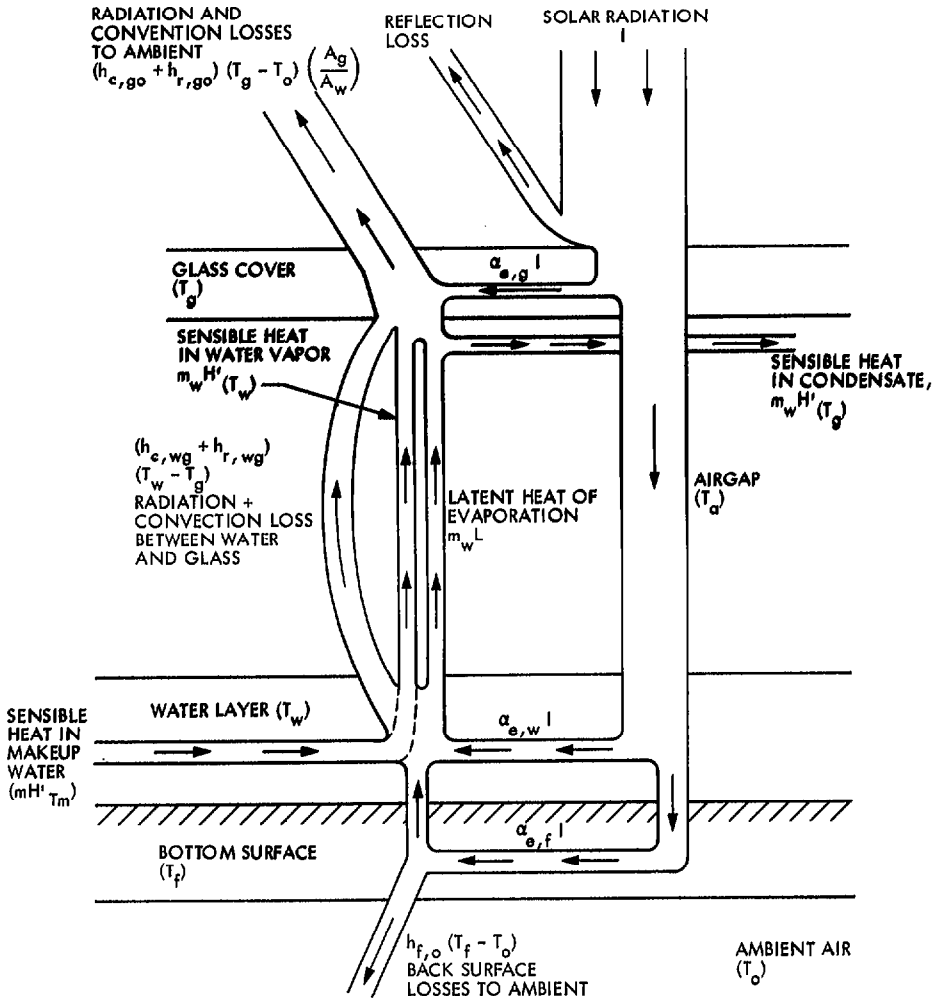

Fig. A-1. Energy flux through still components

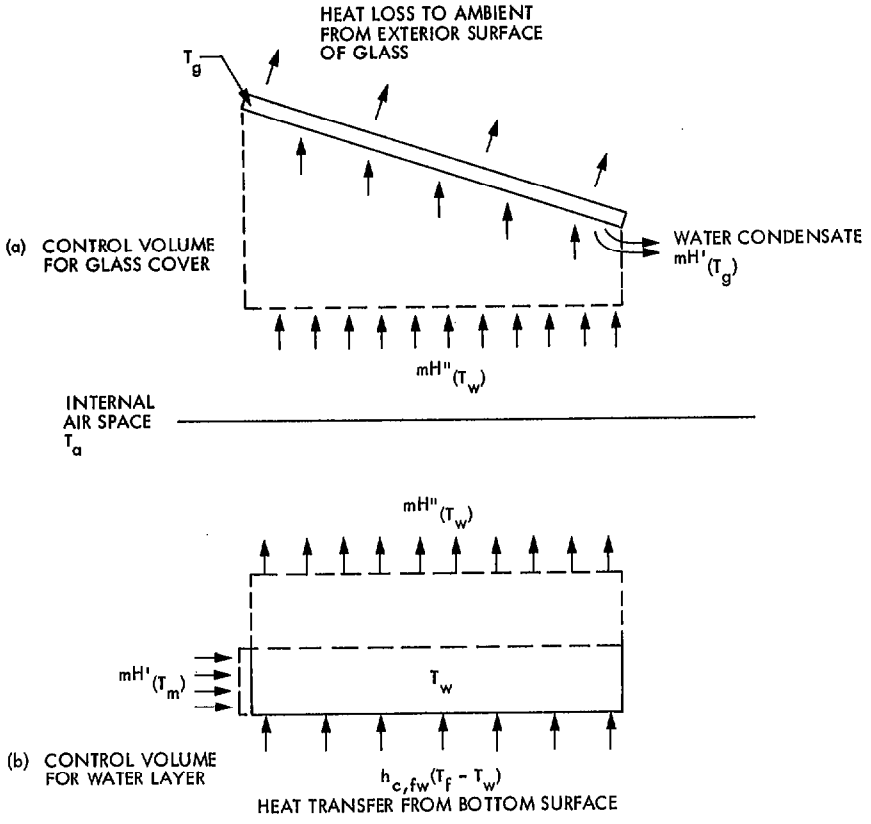

Fig. A-2. Selected control volume for energy equations

Appendix B
Heat Transfer Coefficients

The development of the temperature distribution of the major solar still components as given in Appendix A uses a set of mass transfer, convection, and radiation heat transfer coefficients. The heat transfer coefficients are grouped as follows:

1. Radiation coefficient between glass cover and ambient air $h_{r,go}$. The coefficient $h_{r,go}$ is obtained by linearizing the expression of radiation exchange between the glass cover (taken as a gray surface with emissivity ϵ_g) and a black ambient air (treated as a black body); hence

$$h_{r,go} = \epsilon_g \sigma (T_g^4 - T_o^4)/(T_g - T_o)$$

or

$$h_{r,go} = \xi_g \sigma (T_g^2 + T_o^2)(T_g + T_o) \qquad \text{(B-1)}$$

where σ is Stefan-Boltzmann constant ($= 5.729 \times 10^{-8}$ W/($m^2 \cdot K^4$))

2. Radiation coefficient between glass cover and the water layer $h_{r,wg}$. The radiative coefficient $h_{r,wg}$ is obtained by linearizing the expression of radiation exchange between the glass cover and the water layer, treated as two gray surfaces

$$h_{r,wg} = \epsilon_{wg} \sigma (T_w^4 - T_g^4)/(T_w - T_g)$$

or

$$h_{r,wg} = \epsilon_{wg} \sigma (T_w^2 + T_g^2)(T_w + T_g) \qquad \text{(B-2)}$$

where the effective emissivity ϵ_{wg} is given by Holman (Ref. 8)

$$\frac{1}{\epsilon_{wg}} = \left(\frac{1-\epsilon_g}{a_g}\right)\left(\frac{A_w}{A_g}\right) + \left(\frac{A_w}{A_g F_{wg}}\right) + \frac{1-a_w}{\epsilon_w} \qquad \text{(B-3)}$$

where F_{wg} is the radiation view factor between the water and glass surfaces. Denoting the top, bottom, and side surfaces of the still module as shown in Fig. (B-1) and making use of the view factors expressions between two perpendicular rectangles (Ref. 9),

$$F_{2-4} = \frac{1}{2}\left(1 + \frac{h_4}{w_2} - \sqrt{1 - \left(\frac{h_4}{w_2}\right)^2}\right) \qquad \text{(B-4)}$$

$$F_{2-3} = \frac{1}{2}\left(1 + \frac{h_3}{w_2} - \sqrt{1 - \left(\frac{h_3}{w_2}\right)^2}\right) \qquad \text{(B-5)}$$

since surface 2 does not "see" itself,

$$F_{2-2} = 0$$

$$F_{2-1} = 1 - F_{2-3} - F_{2-4} = F_{wg} \qquad \text{(B-6)}$$

3. Convection coefficient between warm water surface and cold glass cover $h_{c,wg}$. For a horizontal air space enclosed between a warm plate at the bottom and a cold plate at the top, Holman (Ref. 8) gave the natural convection coefficient as:

$$h_{c,wg} = 0.195\, Gr_{\delta a}^{0.25}\, K_a/\delta_a \qquad 10{,}000 < Gr < 400{,}000 \qquad \text{(B-7)}$$

$$h_{c,wg} = 0.068\, Gr_{\delta a}^{0.333}\, K_a/\delta_a \qquad Gr > 400{,}000$$

where $Gr_{\delta a}$ is the Grashof number for the air, δ_a is the thickness of the air space, and k_a is the thermal conductivity of the air evaluated at temperature T_a. k_a in W/m-K is determined by a curve-fitted expression using tabulated data in Ref. 10 as

$$k_a = 0.0003623\, T_a^{0.7488} \qquad \text{(B-8)}$$

The Grashof number is computed with δ_a as the characteristic length by

$$Gr\delta_a = g\beta (T_w - T_g)\, \delta_a^3/\nu_a^2 \qquad \text{(B-9)}$$

where g is the gravitational constant (9.81 m/sec^2), β is the volumetric expansion coefficient (equals $1/T_a$ for an ideal gas at T_a), ν_a is the kinematic viscosity of air (in m^2/sec) evaluated at T_a. An expression for ν_a is obtained, also, by curve-fitting tabulated data from Ref. 10 as

$$\nu_a = 9.253 \times 10^{-10} T_a^{1.709} \quad \text{(B-10)}$$

4. Convection coefficient between the warm bottom surface and the relatively cold water layer $h_{c,fw}$. The average natural convection coefficient between a horizontal flat plate and a liquid is given by Holman (Ref. 8) as

$$h_{c,fw} = 0.27\, k_w (Gr_l Pr_w)^{0.25} / l_w \quad \text{(B-11)}$$

where k_w (in W/m-K) is the thermal conductivity of water evaluated at T_w, l is the characteristic length taken as the mean of the two sides of the rectangular bottom surface of the still, and Pr_w is the Prandtl number for water. By curve fitting tabulated data in Ref. 10 one obtains

$$k_w = 0.557 + 0.0011799\,(T_w - 273.15) \quad \text{(B-12)}$$

and

$$Pr_w = -0.222365 + \frac{200.90503}{(T_w - 273.15)} - \frac{1115.8828}{(T_w - 273.15)^2} \quad \text{(B-13)}$$

The Grashof number of water is computed from

$$Gr_w = 0.00018 g\,(T_f - T_w)\, l^3 / \nu_w^2 \quad \text{(B-14)}$$

where the volumetric expansion coefficient for water β is $0.18 \times 10^{-3}\ K^{-1}$. The kinematic viscosity of water (ν_w) in m^2/sec is determined by curve-fitting tabulated data in Ref. 10 as:

$$\nu_w = 1.1853606 \times 10^{-10} + \frac{32.562357 \times 10^{-6}}{(T_w - 273.15)} - \frac{248.87299 \times 10^{-6}}{(T_w - 273.15)^2} \quad \text{(B-15)}$$

5. Convection coefficient between glass cover and the ambient air $h_{c,go}$. The forced convection heat transfer coefficient $h_{c,go}$ in W/m^2-K is given by Duffie and Beckman (Ref. 11) as

$$h_{c,go} = 5.7 + 3.8V \quad \text{(B-16)}$$

where V is the wind speed in m/sec.

6. Overall heat transfer coefficient from the bottom surface to the ambient air. As shown in Fig. 1, the bottom portion of solar still is composed of three layers: a fiberglass layer, an insulation layer, and a plywood layer. A general expression for the overall heat transfer coefficient h_{fo} through this composite wall can be written as

$$\frac{1}{h_{fo}} = \frac{\delta_i}{k_i} + \frac{\delta_s}{k_s} + \frac{1}{h_{c,fo}} \quad \text{(B-17)}$$

where δ_i and δ_s are the thickness of the insulation and the plywood support, respectively, and k_i and k_s are the thermal conductivity of the insulation and the plywood support, respectively. The convection coefficient between the bottom plywood surface and the ambient air is $h_{c,fo}$.

7. Latent heat of vaporization for water. The latent heat of vaporization expression given by Cooper (Ref. 4) in English units was converted to SI units as

$$L = 883 - 0.6687\,T \quad \text{(B-18)}$$

where T is the absolute water temperature in kelvin and L is given in Whr/kg.

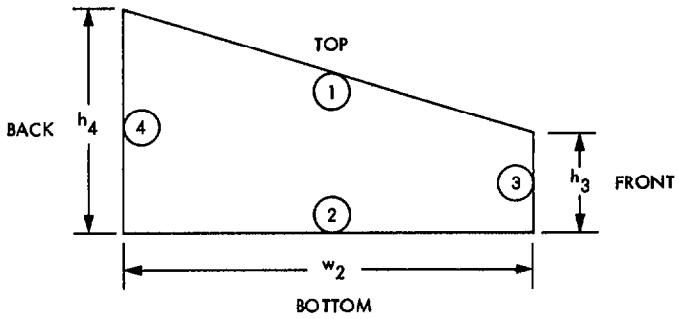

Fig. B-1. Internal solar still radiation view factor

Appendix C
Mass Transfer and Diffusion

The mass transfer is significant in the model since it indicates the water purification rate and consequently the overall efficiency of the solar still. Two approaches for evaluating the mass transfer rate, m_w, are presented as follows:

I. First Approach: Stefan's Law of Diffusion

Following the Stefan's Law of Diffusion (Ref. 8), the total mass flow of water vapor per unit area evaporating from the upper water surface to the still air above is

$$m_{evaporation} = \frac{DPM_w}{\bar{R}\,T_a(\delta_a/2)} \ln \frac{P - P_{wa}}{P - P_{ww}} \qquad \text{(C-1)}$$

where P is the total pressure for air-vapor mixture, $\bar{R}$ is the universal gas constant (8.315 kj/kmol-k), $(\delta_a/2)$ is half the air spacing between the water surface and glazing, D is the water-air diffusion coefficient, T_a is the temperature of air spacing, P_{wa} and P_{ww} are the saturation vapor pressures for water at temperatures T_a and T_w, respectively. Also, for the condensation process at the glazing surface at T_g,

$$m_{condensation} = \frac{DPM_w}{\bar{R}T_a(\delta_a/2)} \ln \frac{P - P_{wg}}{P - P_{wa}} \qquad \text{(C-2)}$$

since at steady-state,

$$m_{condensation} = m_{evaporation} = m_w$$

By eliminating the pressure P_{wa} from Eqs. (C-1) and (C-2) the mass flow m_w for evaporation or condensation at steady state is

$$m_w = \frac{DPM_w}{\bar{R}T_a\,\delta_a} \ln \frac{P - P_{wg}}{P - P_{ww}} \qquad \text{(C-3)}$$

where P_{wg} and P_{ww} are the saturated vapor pressure at temperature T_g and T_w, respectively. An empirical equation for the saturated vapor pressure for water in KN/m^2 or (kP_a) is given by Kays (Ref. 12) from 10°C to 150°C as

$$P_w = 22105.8 \times 10^{-\left[\frac{X(a+bx+cx^3)}{T(1+dx)}\right]} \qquad \text{(C-4)}$$

where T is the saturated water temperature (K) and

$$\left.\begin{aligned} a &= 3.2437814 \\ b &= 5.86826 \times 10^{-3} \\ c &= 1.1702379 \times 10^{-8} \\ d &= 2.1878462 \times 10^{-3} \\ x &= 647.27 - T \end{aligned}\right\} \qquad \text{(C-5)}$$

The diffusion coefficient D between water vapor and air in cm^2/sec is taken from Gilliland's semiempirical relation for any two gases A and B (Ref. 8) as:

$$D = 577.7\,T_a^{3/2} \sqrt{\frac{1}{M_A} + \frac{1}{M_B}} \Big/ [P(\bar{V}_A^{1/3} + \bar{V}_B^{1/3})^2] \qquad \text{(C-6)}$$

where P is the total pressure of the air-vapor mixture in N/m^2, and $\bar{V}_A$ and $\bar{V}_B$ are the molecular volume of A and B. For a mixture of air and water vapor the values of $\bar{V}$ are 29.9 and 18.8, respectively. The molecular weights M for air and water vapor are 28.9 and 18, respectively. At atmospheric pressure $P = 1.0132 \times 10^5$ N/m^2, Eq. (C-6) is reduced to

$$D = 0.04977\,(T_a/100)^{3/2} \qquad \text{(C-7)}$$

Equations (C-3) and (C-7) are combined to give the distilled water production rate m_w in the text.

II. Lewis Number Approach

The mass transfer (or diffusion) of water vapor is the isothermal evaporation of water at T_w and the subsequent diffusion through the stagnant air layer above at T_a. By analogy to heat transfer, the mass transfer per unit surface area is expressed as

$$m_w = h_d(C_w - C_{wa}) \qquad \text{(C-8)}$$

where h_d is the mass transfer coefficient, C_w and C_{wa} are the water vapor concentration (or density $\bar{\rho}$) in saturated air-vapor mixture at temperature T_w and T_a, respectively.

Assuming that water vapor at low pressure follows an ideal gas equation of state, the density $\bar{\rho}_w$ is given by

$$\bar{\rho}_w = M_w P_w/(\bar{R}T) \tag{C-9}$$

where M_w is the molecular weight of water, and P_w is the partial pressure of water vapor in the saturated air layer above; hence

$$m_{evaporation} = h'_d\,(M_w/\bar{R}T_a)(P_{ww} - P_{wa}) \tag{C-10}$$

where h_d is an evaporation mass transfer coefficient, and P_{ww} and P_{wa} are the saturation pressures of water vapor at the temperatures T_w and T_a, respectively. Similarly, the condensation of water vapor taking place at the glass surface at temperature T_g is a result of the concentration difference between water vapor in two saturated air mixtures; one at temperature T_a and the other at a lower temperature T_g. An analogous expression to Eq. (C-10) can be written for the condensing mass rate, as

$$m_{condensation} = h''_d(M_w/\bar{R}T_a)(P_{wa} - P_{wg}) \tag{C-11}$$

where h''_d is the mass transfer coefficient during condensation. At steady state, the make-up water will compensate for the condensate leaving the still; then

$$m_w = m_{evaporation} = m_{condensation}$$

Equating Eqs. (C-10) and (C-11) and eliminating P_{wa}, one obtains the mass flow rate per unit surface area as

$$m_w = M_w(P_{ww} - P_{ww})/\left[\bar{R}T_a\left(\frac{1}{h'_d} + \frac{1}{h''_d}\right)\right] \tag{C-12}$$

Furthermore, if we assume that,

$$h'_d = h''_d = h_d \tag{C-13}$$

where h_d is the mass transfer coefficient at either the interface between the water and air space or between the air space and the glazing, then

$$m_w = (M_w h_d/2\,\bar{R}T_a)\,(P_{ww} - P_{wg}) \tag{C-14}$$

The mass transfer coefficient h_d is obtained following similar relationships between convective heat and mass transfer. These are given by the dimensionaless numbers below:

$$\left.\begin{aligned}&\text{(a) Schmidt number } Sc = \frac{\nu}{D} \text{ in mass transfer}\\ &\text{Prandtl number } Pr = \frac{\nu}{\alpha} \text{ in heat transfer}\end{aligned}\right\} \tag{C-15}$$

and

$$\left.\begin{aligned}&\text{(b) Sherwood number } Sh = \frac{h_d\delta}{D} \text{ in mass transfer}\\ &\text{Nusselt number } Nu = \frac{h_c\delta}{k} \text{ in heat transfer}\end{aligned}\right\} \tag{C-16}$$

where $\bar{\alpha}$ is the thermal diffusivity ($= k/\bar{\rho}\bar{c}$), ν is the kinematic viscosity ($= \mu/\rho$), and D is the diffusion coefficient.

If heat and mass transfer occur simultaneously as is the case in the solar still, the coefficients h_c and h_d are found to be related by Lewis number Le (Ref. 8) as

$$\left.\begin{aligned}h_c/h_d &= \bar{\rho}_a C_a\, Le^{2/3}\\ Le &= \frac{\bar{\alpha}_a}{D} = \frac{Sc}{Pr}\end{aligned}\right\} \tag{C-17}$$

Knowing the value of Lewis number, the physical properties of air-water vapor mixture and the convective heat transfer coefficient h_c will enable the mass transfer coefficient h_d to be computed from Eq. (C-14). This approach was abandoned, however, in favor of the first, simpler, approach which uses direct calculation of the diffusion coefficient D.

Appendix D
Numerical Example

A short computer program was developed to speed up the simulation of a solar still module using the equations presented in Appendices A, B, and C. The total water production rate of the distillation system can be obtained by multiplying the output of one module by the total number of modules in the system.

I. Input Variables

The variables used in the computer program are grouped as follows.

A. Optical Properties

Glass reflection coefficient[1] r_g	0.043
Water reflection coefficient[2] r_w	0.0201
Glass absorption coefficient[3] a_g	0.9730
Water absorption coefficient[4] a_w	0.7065
Bottom surface reflection coefficient[5] b	0.05
Emissivity of water surface ϵ_w	0.9565
Emissivity of glass ϵ_g	0.925
View factor F_{wg}	0.8533

(1) Based on an index of refraction of 1.526.

(2) Based on an index of refraction of 1.33.

(3) Using an extinction coefficient of 6.85 m^{-1} and Eq. (A-3).

(4) Using an extinction coefficient of 6.85 m^{-1} and Eq. (A-3).

(5) Assuming an absorption coefficient of 0.95 for the opaque black-painted bottom.

B. Module Geometry

Average spacing between water surface and the glass cover	6.00 cm
Length of the still base	259.08 cm
Width of the still base	81.28 cm
Height of the front side of the still	8.25 cm
Height of the back side of the still	13.97 cm
Thickness of glass X_g	0.4 cm
Thickness of water layer X_w	5.08 cm
Thickness of fiberglass layer X_f	0.3175 cm
Thickness of insulation X_i	1.905 cm
Thickness of support wood frame X_s	1.905 cm
Surface area of glass A_g	2.111 m^2
Surface area of water A_w	2.1059 m^2

C. Thermodynamic Properties

Prandtl number of air Pr_a	0.7
Conductivity of insulation k_i	0.151 w/m-K
Conductivity of wood k_s	0.2942 w/m-K
Conductivity of fiberglass k_f	0.433 w/m-K
Specific heat of water C_w	1.163 Wh/Kg-K
Total pressure P	97.7 KN/m^2 (KP_a) or 14.2 psi

D. Weather

Solar radiance I	800 W/m^2
Wind speed V	4.47 m/sec (10 mph)
Ambient temperature T_0	299.85 K (80.1°F)

E. Temperatures

Makeup water temperature T_m	299.85 K (80.1°F)

II. Sample Results

The following is a partial list of the results printed by the computer using the input data presented above and the equations given in Appendices A, B, and C.

[1] Based on an index of refraction of 1.526.
[2] Based on an index of refraction of 1.33.
[3] Using an extinction coefficient of 6.85 m^{-1} and Eq. (A-3).
[4] Using an extinction coefficient of 6.85 m^{-1} and Eq. (A-3).
[5] Assuming an absorption coefficient of 0.95 for the opaque black-painted bottom.

A. Optical Properties

Effective absorptivity of glass $\alpha_{e,g}$	0.02805
Effective absorptivity of water $\alpha_{e,w}$	0.26693
Effective absorptivity of bottom $\alpha_{e,f}$	0.58950

B. Thermal Properties

Conductivity of air k_a	0.02787 W/m-K
Conductivity of water k_w	0.6403 W/m-K
Kinematic viscosity of air ν_a	1.8664×10^{-5} m^2/sec
Kinematic viscosity of water ν_w	4.1132×10^{-7} m^2/sec
Prandtl number of water Pr_w	2.3988
Latent heat of evaporation at T_a L_{Ta}	662.15 Whr/kg
Saturated vapor pressure at T_g P_{wg}	8.91133 KN/m^2
Saturated vapor pressure at T_w P_{ww}	31.9833 KN/m^2

C. Heat Transfer Coefficients

Radiation coefficient between glass cover and ambient air $h_{r,go}$		6.2165 W/m^2-K
Radiation coefficient between water layer and glass cover $h_{r,wg}$		6.3690 W/m^2-K
Forced convection coefficient between glass cover and ambient air $h_{c,go} = h_{c,fo}$		22.686 W/m^2-K
Natural convection coefficient between water layer and glass cover $h_{c,wg}$		2.503 W/m^2-K
Overall heat transfer coefficient between the bottom surface and the ambient air h_{fo}		4.25549 W/m^2-K
Natural convection coefficient between the bottom surface and the water layer, $h_{c,fw}$		81.245 W/m^2-K
Combined heat transfer coefficients:	B_1	28.9725 W/m^2-K
	B_2	8.8717 W/m^2-K
	B_3	90.5190 W/m^2-K
Equivalent coefficient:	B_4	85.5011 W/m^2-K

D. Temperatures

Glass cover temperature T_g	317.1 K
Water layer temperature T_w	343.8 K
Bottom surface temperature T_f	347.2 K

E. Performance

Water production rate per module	0.727 kg/hr
Quasi-steady-state efficiency	28.6%

From the energy balance equations presented in Appendix A, an energy flux distribution of the solar still can be developed. Figure D-1 shows the energy flux through the module. Assuming that 100 units of solar energy are radiated upon the still projected surface, 11.6 units of energy will be reflected back to the ambient air. The glass cover absorbs 2.8 units of energy and transmits the remaining 85.6 units to the still interior. The water layer absorbs 26.7 units of energy and the remainder is absorbed by the bottom surface. The makeup water for this example contributes 0.9 units of sensible heat loss from the solar still. The thermal loss of the top surface is more than twice that of the bottom. The back loss could be reduced further if the still is better insulated.

Water distillation rate depends mainly on incident solar radiation. To investigate this effect, the ambient temperature T_0 was kept constant at 26.7°C (299.85 K) and several simulations were made using various solar intensities. The results are illustrated in Fig. D-2, showing a nonlinear relationship between the solar radiation intensity and the water purification rate. At 200 W/m^2 solar intensity the water distillation rate is approximately 0.05 kg/(hr-m^2), which increases to 0.35 kg/(hr-m^2) at 800 W/m^2. The water distillation sensitivity is accelerated as the solar radiation becomes higher than 400 W/m^2. Since the average daily solar radiation is higher in summer than in winter, the water distillation rate will be high in summer and low in winter, as shown in Fig. D-2.

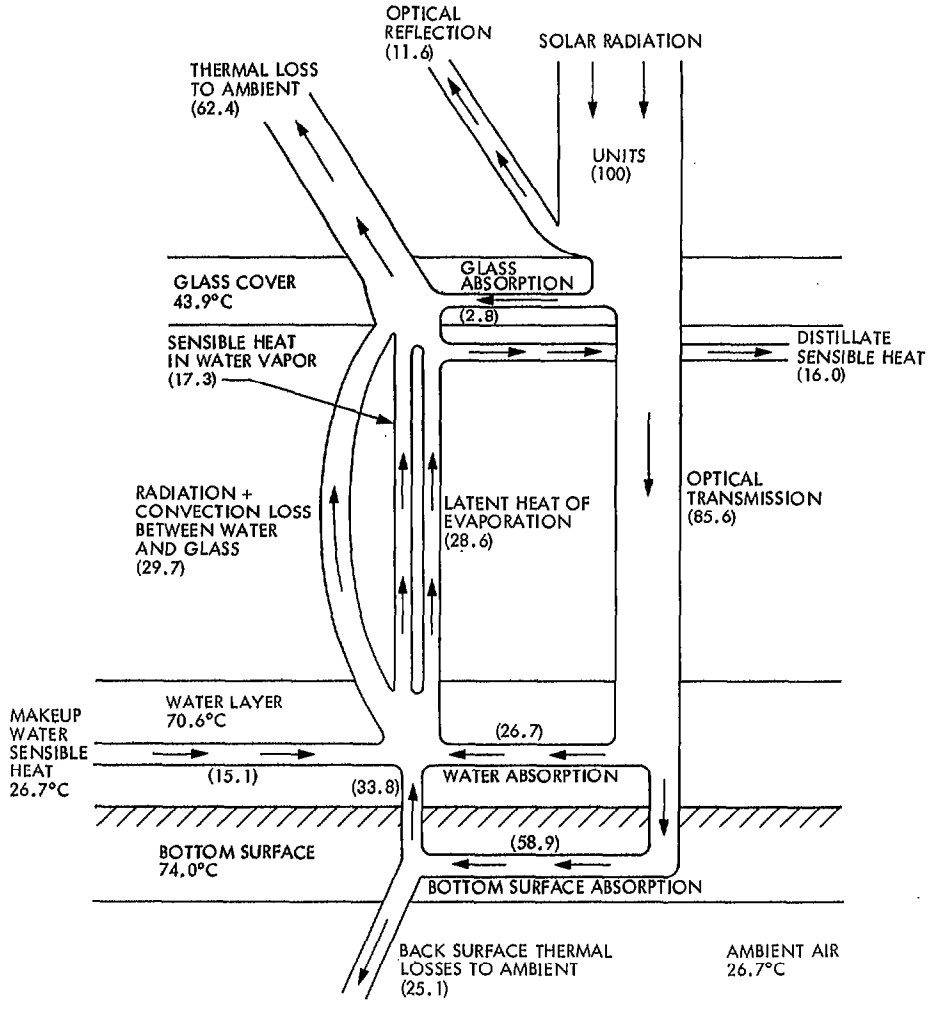

Fig. D-1. Energy flux through still components for the sample 1-hour simulation

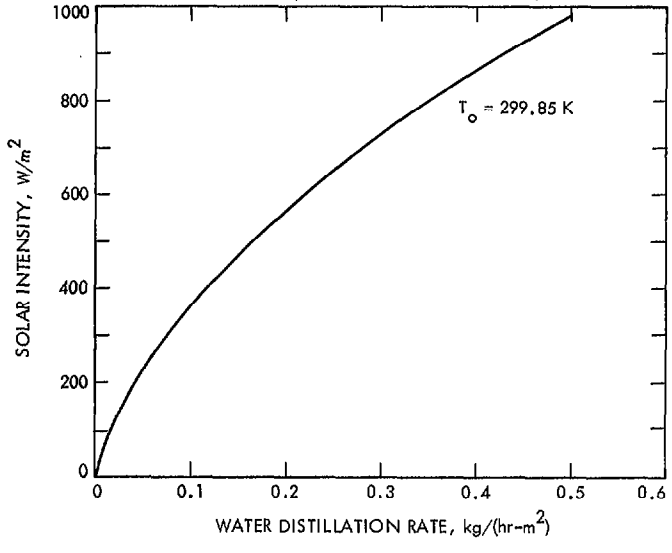

Fig. D-2. Solar radiation versus water distillation rate